Physical and mathematical problems of 1D modelling of transonic two-phase flow in a convergent-divergent nozzle

Wojciech Angielczyk

Bialystok University of Technology, 45A Wiejska Street, 15-351 Bialystok, Poland
Author email: w.angielczyk@pb.edu.pl

Abstract

This work addresses the challenges associated with one-dimensional modelling of steady transonic two-phase flows illustrated through simulations of selected flow cases of the famous Moby Dick experiment. It primarily concentrates on the method for a fast determination of the transonic trajectory. The second proposed approach allows for determining trajectories describing the transonic flow with a normal shock wave. The first method is successfully verified by comparing its results with simulation results obtained from the (widely known and thoroughly verified) Wavefront Algorithm for High-speed Aerodynamics code, utilizing the Delayed Equilibrium Model. The first method mentioned is the author's proposition that is competitive to conventional (time-expensive) approaches such as the Newton Critical Point or achieving a steady flow description by asymptotical convergence of the time-dependent model's solutions, and it is a completely new consistent solution method. The second proposed method is an adaptation of the Rankine–Hugoniot jump conditions to a two-phase flow described by the Delayed Equilibrium Model. In the case of this method, the presented here analysis and results serve only as a proof of concept. Similar methods have been described before, but the results presented in this article, obtained with the Delayed Equilibrium Model, are unique. Also, a limited but coherent model of thermodynamic properties of a superheated liquid is presented and physically justified. This model was formulated earlier and is often used, but its comprehensive derivation has not been presented before.

Keywords: Transonic trajectory; Steady two-phase flow; Normal shock; Moby Dick experiment; Metastable liquid

1. Introduction

Flows encountered in machines and industry can be frequently classified as steady-state. These flows can be simulated using three-dimensional (3D) models of unsteady flow. Consequently, it may appear that current Computational Fluid Dynamics (CFD) methods adequately address the needs of designers, engineers and researchers. However, in practice, such methods are rarely employed at the initial stages of the flow analysis or description. This is mainly due to the extensive computational time required for CFD simulations with today's available computing

speed. The simulations are even more challenging when the fluid velocity magnitude passes through the value of the local sound speed [1]. Moreover, certain characteristics of the flow can only be evaluated through an analysis of the time-independent version of the model [2]. As a result, fast one-dimensional (1D) transonic steady-state approaches remain essential.

This article, therefore, reintroduces a fast general method of transonic trajectory determination (TTD) that is competitive with conventional time-consuming approaches (such as the Newton Critical Point [3] or asymptotical convergence of time-dependent solutions [4]). The method has been developed by the

Angielczyk W.

Nomenclature

A – cross-section area of the flow channel, m^2

$\mathbf{A}$ – main matrix of the governing equation system

$\boldsymbol{b}$ – vector of the source terms

C – perimeter of the flow channel, m

c_p – specific heat at constant pressure, J/(kg K)

h – specific enthalpy, J/kg

l – dummy parameter

M – mass flow rate, kg/s

n – size of the velocity-state vector

p – absolute static pressure, MPa

q – heat flux, J/(s m^2)

r – channel radius, m

s – specific entropy, J/(kg K)

t – static temperature, ºC

T – absolute static temperature, K

v – specific volume, m^3/kg

$\boldsymbol{V}$ – vector tangent to the trajectory

w – velocity, m/s

x – saturated vapour mass fraction

y – saturation index

z – spatial coordinate, m

Greek symbols

α – void fraction

ρ – mass density, kg/m^3

$\boldsymbol{\sigma}$ – velocity-state vector

τ – shear stress, Pa

Ω – phase space

Subscripts and Superscripts

0 – intersection point of the subcooled liquid expansion curve with the saturated liquid line

B – flow channel inlet

c – critical

$calc$ – calculated

exp – experimental

IN – nozzle inlet

$onset$ – nucleation onset

sat – saturation

T – throat

w – wall

Abbreviations and Acronyms

CFD – computational fluid dynamics

DEM – delayed equilibrium model

HEM – homogeneous equilibrium model

HRM – homogenous relaxation model

IF – impossible flow

NCP – Newton critical point

PF – possible flow

PIF – possible-impossible flow

SMD LN – Super Moby Dick Long Nozzle experiment

TTD – transonic trajectory Determination

WAHA – wavefront algorithm for high-speed aerodynamics

author in a previous paper [5] but appears to be underappreciated and underutilized. This could be since in its original presentation [5] only the mathematical proof of its validity was given. Hence, this paper provides a more practical demonstration of the method's correctness. Namely, a confrontation of results obtained by application of the mentioned method with results obtained from the well-known Wavefront Algorithm for High-speed Aerodynamics (WAHA) code [6], utilizing the Delayed Equilibrium Model (DEM). To verify the method, selected flow cases of the Moby Dick experiment [7] were simulated and analysed.

The DEM was chosen because it is sufficiently complex in some mathematical aspects (the 5-component velocity-state vector) allowing for a demonstration of the method's universality. Moreover, previous studies have shown that it aligns closely with the subsonic results of the Moby Dick experiment, with excellent predictivity of the critical mass flow rate [8]. Nonetheless, any other two-phase homogeneous relaxation flow model could serve equally well for verification purposes [5]. In turn, the results of simulations using the WAHA code were selected as reference data, because the code has undergone extensive experimental validation [9]. Furthermore, simulations of the Moby Dick experiment conducted with the WAHA code were provided by the authors of the article [8].

The first known to the author attempts at formulating a general approach for Transonic Trajectory Determination (TTD) were conducted in the 1960s [10]. The cited report presents an approach, called the "optimum-point method", dedicated to single-equation nozzle flow models, including those with nonequi-

librium. However, single-equation flow models are generally too simplistic to accurately capture phenomena in flows other than gases. Consequently, this method lacks the generality needed for broader applications. The same report briefly describes other approaches but all of them focus on highly simplified models. In the late 1980s, significant advancements in TTD were made when the methodology of dynamical systems theory was successfully applied to a broad class of mathematical models describing 1D two-phase flows [2]. It was demonstrated that the direction of the transonic trajectory at the singular point can be determined using the aforementioned theory. This result was crucial for applying the shooting method to solve the initial-value problem (see Section 3). However, the models studied and the assumptions made, simplified the problem to the extent that the applied solution algorithms cannot be considered general methods. Subsequent work has tackled more complex flows, incorporating factors such as heat transfer between the fluid and the environment and friction effects. For instance, in [11], a version of the Newton Critical Point (NCP) method was applied to solve the compressible Euler equations, including gravity and heat source terms. While the method demonstrated speed and accuracy, this performance might be attributed to the simulations being limited to perfect gas flows without friction effects. Simultaneously, several codes were developed to describe 1D unsteady two-phase flows, including: RELAP5, TRAC, CATHARE, TRACE and WAHA. RELAP5 is a thermal-hydraulic simulation code developed for analysing flows and accidents related to light water nuclear reactor systems [12]. TRAC is a thermal-hydraulic code, devoted to nuclear reactor flows in general,

capable of handling non-equilibrium conditions [13]. CATH-ARE is an approach based on a six-equation two-fluid model, designed for reactor safety and accident analysis [14]. TRACE is a thermal-hydraulic simulation tool with multidimensional modelling capabilities, aimed at safety analysis of nuclear reactors [15]. WAHA is a 1D thermal-hydraulic code based on a six-equation two-fluid model for modelling transient flows such as water hammer and pressure wave propagation phenomena in piping systems [16]. It is capable of handling non-equilibrium conditions and flexible channels. RELAP5, CATHARE and WAHA are strictly 1D approaches while the remaining codes allow for 2D and 3D analysis. All the mentioned codes are transient flow approaches. Therefore, in the following years, the methods of solving the considered problems were dominated by the use of unsteady flow models in which the steady-state solution was obtained in asymptotic convergence of the transient-flow solutions. Although it was both practically verified and analytically demonstrated [17] that these traditional time-marching methods converge slowly. The most recent works, in which TTD did not involve the use of transient flow models, were conducted by teams that included the author of this paper. In [5], the developed methods were applied to modelling two-phase carbon dioxide flows. The determination of the critical mass flow rate in two-phase carbon dioxide flows using DEM and the Homogeneous Equilibrium Model (HEM) was investigated in [18]. Then, a development of the DEM was described in [19]. In these two papers, the methods proposed here were applied. In the most recent publication [20], the author critically analysed the relaxation equations used in modelling multiphase transonic flows. Admittedly, the proposed methods were not used, but many of the author's insights that emerged during the methods' development were applied.

The second proposed approach adopts the Rankine–Hugoniot jump conditions in a two-phase flow described by the DEM to predict the normal shock wave (that may potentially occur in the flow) and the trajectory following the shock. Thus, the proposal may be seen as not particularly innovative; However, to the best of the author's knowledge, this approach has only been theoretically outlined in the context of 1D modelling of steady transonic two-phase flows using the HEM and the Homogeneous Relaxation Model (HRM) [1]. More practically, in the context of the two-phase flows, it was investigated only in [21], but also with the application of a very simplistic model. Certainly, a similar method has not been used with the DEM. Furthermore, aside from this work, no practical (implementation-oriented) description of a comparable method has been published. This gap in the literature presents a unique opportunity to explore the method's applicability, which could lead to valuable insights into the research domain.

Nevertheless, the behaviour of normal shocks has been frequently investigated using transient models. For example, in [22], the WAHA code was applied to simulate the Moby Dick experiment flows that often contained a shock wave. Also, CFD methods were applied in similar kinds of simulations. For instance, the significant challenge of capturing shocks in steam turbines was addressed in [23]. In [24], the developed CFD model was successfully validated against the non-equilibrium

condensation in Gyarmathy's nozzle under high-pressure conditions. Moreover, condensation-induced shock waves were well captured by this model. In [25], based on a CFD analysis, the Laval nozzle was designed to give a more significant pressure drop than a conventional nozzle by eliminating the shock wave strings at the nozzle throat.

2. The two-phase flow model and the submodels

2.1. Delayed Equilibrium Model

Due to the reasons explained in the introduction, the DEM was chosen to simulate the selected flow cases of the Moby Dick experiment. The DEM assumes the existence of three fractions, although it is treated as a two-phase model. Those fractions are the metastable liquid phase (subscript ML), the saturated liquid phase (subscript SL), and the saturated vapour phase (subscript SG). The metastable fraction is assumed to have the same pressure as the saturated phases but higher temperature, as it is assumed to undergo an isentropic expansion. Therefore, the DEM takes into account the thermal non-equilibrium effects, but it does not include the mechanical non-equilibrium effects (the velocities of the phases are equal since they are perfectly mixed – a homogenous mixture). The model consists of three conservation equations of mass, momentum, and energy, and two state equations (describing specific volume v and the specific enthalpy h), respectively:

$$w\frac{d\rho}{dz} + \rho\frac{dw}{dz} = -\rho w\frac{1}{A}\frac{dA}{dz}, \qquad (1)$$

$$\frac{dp}{dz} + \rho w\frac{dw}{dz} = -\frac{\tau_w C}{A}, \qquad (2)$$

$$\rho w\frac{dh}{dz} - w\frac{dp}{dz} = w\frac{\tau_w C}{A} + \frac{qC}{A}, \qquad (3)$$

$$v = \rho^{-1} = (1-y)v_{ML} + (y-x)v_{SL} + xv_{SG}, \qquad (4)$$

$$h = (1-y)h_{ML} + (y-x)h_{SL} + xh_{SG}. \qquad (5)$$

Those equations describe a flow in a horizontal channel of variable cross-section area and contain the following quantities associated with the flowing two-phase mixture: p – the absolute static pressure, v – the specific volume, ρ – the mass density, w – the velocity, h – the specific enthalpy, x – the saturated vapour mass fraction, y – the saturation index. As well as the geometrical parameters of the flow channel (A – the cross-section area, C – the perimeter) that are functions of the spatial coordinate z measured from the channel inlet along its axis. Finally, τ_w is the wall shear stress (determined from the Lockhart-Martinelli model) and q is the heat flux. However, the last one is assumed to be zero since the flows in the transonic nozzle are treated as adiabatic.

The saturation index is defined as follows:

$$y = \frac{M_{SG}+M_{SL}}{M_{SL}+M_{SG}+M_{ML}} = \frac{M_{SG}+M_{SL}}{M} = x + \frac{M_{SL}}{M}, \qquad (6)$$

where M stands for the two-phase mixture mass flow rate (the remaining M_S with appropriate subscripts stand for mass flow rates of the considered phases).

To complete the model, a mass balance equation for saturated fractions must be added to the system of Eqs. (1−5, 7). This closure equation has been developed for water [26] in the following form:

$$\frac{dy}{dz} = \left(C_1 \frac{c}{A} + C_2\right)(1 - y)\left[\frac{p_{sat}(T_{ML}) - p}{p_c - p_{sat}(T_{ML})}\right]^{C_3}, \quad (7)$$

$C_1 = 0.008390$, $C_2 = 0.633691$ m^{-1}, $C_3 = 0.228127$.

In the above relation, p_{sat} is the saturation pressure at the metastable liquid water temperature T_{ML} and p_c is water's critical pressure.

2.2. Metastable liquid thermodynamic properties model

The flow model presented in the previous section contains the thermodynamic variables of the metastable liquid phase, namely: v_{ML}, h_{ML} and T_{ML}. Therefore, it is required to formulate a submodel describing these quantities. Below, such a submodel is formulated. In fact, it is a simplified and limited version of the metastable liquid phase thermodynamic properties model, but it is consistent, simple, fast and clearly explained.

The specific enthalpy of the metastable fraction can be modelled based on the first law of thermodynamics in the form: $dh = vdp + Tds$ (s stands for the specific entropy). This form needs to be integrated from conditions determined by the intersection point of the subcooled liquid expansion curve with the saturated liquid line, up to conditions given by the mixture pressure p and temperature of the metastable liquid T_{ML}. If the properties in the mentioned intersection point are denoted with subscript 0 then the specific enthalpy of the metastable fraction is given by the following formula:

$$h_{ML}(p, T_{ML}) = h_0 + \int_{p_0}^{p}\left(v_{ML} + T_{ML}\frac{ds_{ML}}{dp}\right)dp. \quad (8)$$

It is worth noticing that calculation of the specific enthalpy, with the above formula, requires utilization of a metastable liquid state equation to determine v_{ML} for given p and T_{ML}. As well as, additional assumptions/relations for calculating T_{ML} and ds_{ML}/dp. In this investigation (as in many others studies, e.g. [27,28]) it was assumed that the metastable liquid fraction is subjected to an isentropic expansion (thus $ds_{ML}/dp = 0$) and that it is incompressible:

$$v_{ML} = v_0, \quad (9)$$

as a result, the metastable fraction specific enthalpy is a function of only pressure:

$$h_{ML}(p) = h_0 + \int_{p_0}^{p} v_0\, dp = h_0 + v_0(p - p_0). \quad (10)$$

In order to obtain an expression for T_{ML}, let us analyse the process starting from the state 0 by applying the first law of thermodynamics in the following way:

$$T_0\, ds = dh - v_0\, dp = k\, c_{p,0}\, dT - v_0\, dp, \quad (11)$$

where k is a correction factor that allows one to include the deviation of the considered process from the isobaric process. In

the case of an ideal gas, the value of k is one, and the specific heat at constant pressure $c_{p,0}$ is constant. For simplicity, let us approximate the behaviour of the metastable liquid by those assumptions. Then, in the isentropic flow, the metastable liquid temperature is given by the following equation:

$$T_{ML} \approx T_0 + \int_{p_0}^{p}\frac{v_0}{c_{p,0}}dp = T_0 + \frac{v_0}{c_{p,0}}(p - p_0). \quad (12)$$

2.3. Nucleation onset

Finally, the pressure at which nucleation in the metastable fraction starts must be specified. It should be noted that this quantity is decisive for the application of a metastable liquid flow model or a two-phase flow model. However, it may be related to the metastable liquid existence limits, which are determined based on the metastable liquid properties model [29]. Here, a simple approach is adopted (in order to be consistent with the WAHA code simulations), assuming that it is a function of the fluid temperature at the channel inlet T_{IN}:

$$p_{onset} = 0.965\, p_{sat}(T_{IN}). \quad (13)$$

2.4. Summary

Incorporating Eq. (4) and Eq. (5) into Eqs. (1−3), and then including Eq. (9) and Eq. (10) in the resulting system and Eq. (12) in Eq. (7), we derive a practical (ready for implementation) formulation of the model. This formulation consists of the equations for the conservation of mass, momentum, energy, and the closure Eq. (7), and it includes only the following gradients: $dA(z)/dz$, dp/dz, dx/dz, dy/dz, dw/dz, $dv_{SL}(p)/dz$, $dv_{SG}(p)/dz$. The first gradient is determined entirely by the flow channel geometry, while the last two depend solely on p. Moreover, in the applied Lockhart-Martinelli model $\tau_w = \tau_w(p, x, y, w)$, while A and C are functions of z. Thus, the practical formulation comprises four equations with four independent variables, which are the gradients of pressure p, vapour mass fraction x, saturation index y, and fluid velocity w.

3. Topological aspects of the modelling and conventional solution procedure

In a case where the flow channel inlet is fed with fluid/liquid in its supercritical, subcooled or metastable state, a single-phase flow model must be applied before a two-phase flow approach. The single-phase flow model consists of Eqs. (1)−(3) supplemented with state equations describing the supercritical, subcooled or metastable liquid properties. These governing equations operate until the nucleation onset. Subsequently, a two-phase flow model should be applied.

As long as the expansion goes from the supercritical state through subcooled and metastable liquid states the fluid compressibility remains low, ensuring that the flow is subsonic. Consequently, the single-phase flow model solutions could be determined by conventional forward-marching integration of the governing equations' system. However, the determination of the transonic solution of the DEM (or other two-phase flow models) is not that simple. It requires an in-depth topological analysis based on the dynamical systems theory, as conducted by Bilicki

et al. [2]. Below, only the essential elements of that analysis are presented, which are necessary to understand the foundation of conventional solution procedure as well as the proposed (in the next section) fast method.

3.1. General and autonomous form of the governing equation system

Practically all known one-dimensional models of a steady-state flow can be presented in the form of the following nonlinear ordinary first-order differential equation system [2]:

$$\mathbf{A}(\boldsymbol{\sigma})\frac{d\boldsymbol{\sigma}}{dz} = \boldsymbol{b}(z, \boldsymbol{\sigma}). \tag{14}$$

The size and elements of the matrix $\mathbf{A}$ and the vector $\boldsymbol{\sigma}$ depend on the model type. The vector $\boldsymbol{\sigma}$ consists of n quantities describing a thermodynamic state of the fluid, and if necessary, the velocity of the fluid (in this case it is called the velocity-state vector). The elements of the matrix $\mathbf{A}$ depend only on $\boldsymbol{\sigma}'$s components, and $\boldsymbol{b}$'s elements additionally depend on the spatial coordinate z. The set of governing Eqs. (14) supplied with the vector $\boldsymbol{\sigma}_{\mathrm{B}} = [\sigma_{1,\mathrm{B}}, \sigma_{2,\mathrm{B}}, \ldots, \sigma_{n,\mathrm{B}}]$ (describing the flow inlet conditions, the inlet is located at z_B) creates an initial-value problem. A solution to the problem is a trajectory $\boldsymbol{\sigma}(z)$ in $n + 1$ dimensional phase space Ω, an approximation of which can sometimes be obtained by numerical integration of the equation system (14).

The system of Eqs. (14) can be solved with respect to the derivatives of $\boldsymbol{\sigma}$'s components by using Cramer's rule:

$$\frac{d\sigma_i}{dz} = \frac{N_i(z,\boldsymbol{\sigma})}{D(\boldsymbol{\sigma})}, \qquad i = 1, 2, \ldots, n, \tag{15}$$

where D denotes the determinant of $\mathbf{A}$, and N_i are determinants, each of which is created by replacing the i-th column of $\mathbf{A}$ with $\boldsymbol{b}$. The most practically useful form of the equation system is obtained by application of the dummy parameter l:

$$\frac{dz}{dl} = D, \qquad \frac{d\sigma_i}{dl} = N_i. \tag{16}$$

It is worth noticing that in the above autonomous form, the independent variable is not z but the dummy parameter l.

To complete this part, it should be noted that, in accordance with the previous section, the applied DEM uses a 5-component velocity-state vector defined as follows:

$$\boldsymbol{\sigma} = [z, p, x, y, w]. \tag{17}$$

3.2. Topological structure of the phase space

Each possible state of a system is represented as a point in the phase space Ω. For example, if in the mathematical model $n = 3$, then $\boldsymbol{\sigma}$ consists of three components—say, pressure p, enthalpy h, and velocity w. Consequently, the state of the fluid and flow in any cross-section of the flow channel is determined by the values of these three parameters, along with the spatial coordinate z. Thus, in this example, the phase space is 4-dimensional. In general, however, the phase space is $n + 1$ dimensional. For simplicity, the most interesting features of its structure are presented as projections onto the pressure p – spatial coordinate z plane, as shown in Fig. 1.
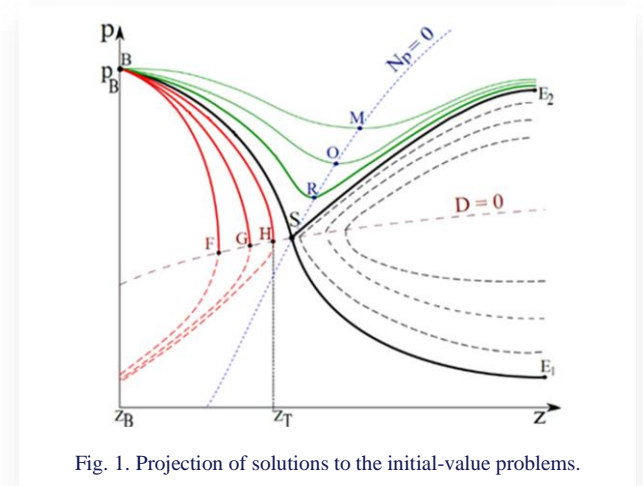
Fig. 1. Projection of solutions to the initial-value problems.

Accordingly, the black, green and red curves present projections of $n + 1$ dimensional trajectories on the $p-z$ plane. Each solid line is a projection of a solution to the initial-value problem mentioned in the previous subsection. The inlet conditions related to those flows differ only in the velocities. Consequently, all trajectories related to the solid lines start from the same values of the inlet pressure p_B, inlet density ρ_B and inlet specific enthalpy h_B but they are related to different mass flow rates.

Three distinct classes of points in the phase space must be distinguished:

1. **Regular points** at which $D \neq 0$. At each of these points, equation systems (14), (15) and (16) are equivalent. Any numerical forward-marching integration of system (14) starting from the inlet conditions $B = [z_B, \sigma_{1,B}, \sigma_{2,B}, \ldots, \sigma_{n,B}]$ and proceeding toward the channel outlet through only the regular points, provides an appropriate approximation to a physically acceptable analytic solution. At such points, system (14) satisfies the existence and uniqueness requirements (only one trajectory passes through any regular point). A trajectory consisting of only regular points is fully subsonic or fully supersonic. Figure 1 shows projections of three subsonic trajectories – the green curves. They are called Possible Flow (PF) trajectories.

2. **Turning points** at which $D = 0$ and all $N_i \neq 0$. At those points, the systems (14) and (15) are not equivalent. Numerical integration of (14), in the vicinity of the turning point, produces a systematically accumulating numerical error. As a result, the integration could become impossible even before reaching the turning point. This is because $|d\sigma_i/dz| \to \infty$ while $D \to 0$. However, the autonomous system (16) satisfies the existence and uniqueness requirements at those points. Hence, during its numerical integration, one can simply pass through a turning point and can obtain a proper approximation of a trajectory that, at the turning point, changes direction along the z-axis (the red curves in Fig. 1). The one-dimensional steady-state flow cannot change direction in the channel. Therefore, those trajectories are physically acceptable only if they pass through a point of inlet conditions B and the turning point is located at the end of the channel. Consequently, the solutions that pass through turning points localized inside of the channel are called Im-

145

possible Flow (IF) trajectories.

In work [1], it was shown that $D = 0$ occurring at the channel end is also a choking criterion (or critical flow condition) since $D = 0$ means that at this point the fluid's velocity reaches the local speed of sound, and as a result, the mass flow rate and the subsonic part of the trajectory are unchangeable even despite a possible pressure drop occurring beyond the channel exit.

Figure 1 shows a projection of three IF trajectories (the red curves). They pass through the turning points F, G, H. Turning points determine the curve $D = 0$ (the projection of this curve is shown in Fig. 1 as the brown dashed line).

3. **Singular points** at which $D = 0$ and all $N_i = 0$. Here are considered only nondegenerate singular saddle points like S at which rank $(\mathbf{A}) = n - 1$ and through which exactly two trajectories pass. Namely, B-S-E$_1$ and B-S-E$_2$ in Fig. 1 (but only B-S-E$_1$ is "really" a transonic trajectory since on B-S-E$_2$ the velocity of the fluid reaches the speed of sound merely at point S to decrease just after it [1]).

According to Eq. (16), $dz = Ddl$ and $d\sigma_i = N_i dl$. Therefore, at those points, finite changes Δz and $\Delta\sigma_i$ calculated by the numerical methods are equal to 0 regardless of the integration step size Δl. It means that the numerical algorithms cannot neither "start from" nor "pass through" this kind of points (they simply "get stuck" in these points - in the theory of differential equations, such points are called equilibrium points). Therefore, contrary to remaining trajectories, the transonic trajectory cannot be determined by a conventional numerical forward-marching integration (even of the system 16).

In [1], it was shown that when $D = 0$ and an arbitrary $N_i = 0$ then all remaining Ns also vanish.

3.3. Conventional solution method - NCP

Formally, NCP is a shooting method that starts from singular saddle points and uses the multidimensional, globally convergent Newton-Raphson algorithm to fit into given inlet conditions [11]. The general concept can be described in 4 steps:

1. Guess a singular saddle point coordinates.
2. Find the transonic trajectory passing through the singular saddle point (or at least, its subsonic part and related inlet conditions).
3. Calculate the deviation of the found solution at the channel inlet from the desired inlet values.
4. Figure out how to change the guessed singular point parameters (using the Newton-Raphson algorithm) to decrease the deviation calculated in the previous step.

Those steps are repeated until the aforementioned deviation is sufficiently low.

The above description (however excellent in describing the general concept) does not illustrate the enormous overall numerical operations number, and as a result, the huge time consumption connected with conducting the NCP procedure. The computation time is so high mostly due the step 4. This issue is extensively explained by the author in [30].

Nevertheless, NCP is still faster and more accurate than the asymptotical convergence to a steady state solution of the unste-
ady model solutions [11].

3.4. Possible-Impossible Flow algorithm

In fact, the Possible-Impossible Flow (PIF) algorithm is not able to determine the transonic trajectory related to given inlet conditions. Thus, it cannot be treated as a solution procedure for the problem considered. However, it is very fast and can be used as a preliminary step towards the solution. Since, with each PIF iteration, the region of phase space that contains the subsonic part of the sought trajectory is narrowed down. Thus, this trajectory part could be localized in an arbitrarily small region of the phase space (however, in practice, the numerical errors preclude restricting the region arbitrarily). The idea of PIF is based on the fact that the sought transonic trajectory lies between PF and IF trajectories (Fig. 1). As it was mentioned earlier, those trajectories can be easily obtained by numerical forward-marching integration of the equation system (16). The PIF algorithm has been widely used, for instance by Bouré et al. [31], or more recently by Lorenzo et al. [28] in the form that can be described in the following steps:

1. Calculate an intermediate mass flow rate $M = (M_{PF} + M_{IF})/2$ and related inlet velocity w.
2. Integrate system of Eqs. (16) from the inlet conditions and at each step, check if D has changed the sign.
3. If D has changed its sign before the end of the channel, then assign the value of M to M_{IF}. If D has not changed its sign before the end of the channel, then assign the value to M_{PF}.
4. If $(M_{IF} - M_{PF})$ is low enough then stop, otherwise go to point 1.

As a result of conducting the PIF algorithm, we obtain two values of the mass flow rate that are, respectively, the upper and lower limit for the critical mass flow rate. Similarly, we get two trajectories (IF and PF) that restrict the phase space to the region containing subsonic part of the sought transonic trajectory. Those "border" trajectories share with the transonic trajectory all values of the inlet parameters excluding velocity. The data obtained as a result of conducting the PIF algorithm are a basis for application of the fast transonic trajectory determination approach that is proposed in the next section.

In [30], the author proposed an even faster-converging version of the PIF algorithm.

4. Proposition of fast transonic trajectory determination approach

It is worth noting that the concept of a general procedure leading to TTD was initially, albeit imprecisely, introduced as early as in 1964 [10]: „The singularity problem can also be attacked by means of trial-and-error procedures, wherein numerous integrations are performed, each with a slightly different value for the mass flow (...). Once a subsonic solution is available that is sufficiently close to the critical one, the integration can then be started from a supersonic initial point obtained by extrapolating the subsonic solution across the singularity". The mentioned trial-and-error procedure is described in the previous subsection as the PIF algorithm, which at that time was not referred to by this name. However, the final step of the above procedure,

namely the extrapolation of the subsonic solution across the singularity, is the tricky part. It is crucial to precisely determine the point of the subsonic trajectory to start the extrapolation. From Fig. 1, it is evident that extrapolation from point R (or any point to its right) would fail, as it would result in a clear discontinuity in the obtained trajectory (or subsonic trajectory). Moreover, to extrapolate 'across the singularity' it is necessary to know where the singularity is located (the PIF algorithm does not localise it), and what 'across' means. Unfortunately, the author of [10] did not clarify those issues. He believed the approach would require a 'considerable consumption of computer time' and abandoned it. Instead, he developed a significantly less general method (briefly described in the introduction). In this section, not only are the 'mystery points' clearly identified and the procedures for their determination described, but also explanations are provided that refer to the previously characterized structure of the phase space and the initial-value problem, complementing and enhancing the aforementioned concept.

The proposed fast TDD method can be divided into four stages:

1. Conduction of the PIF algorithm in order to obtain approximations of trajectories around the singular saddle point.
2. Utilization of the obtained data for determination of the singular saddle point coordinates.
3. Determination of the direction of the transonic trajectory at the singular saddle point from the obtained data.
4. Integration "from" the singular point up to B and down to E_1.

4.1. Generalised method of singular saddle point determination

The proposed method utilises the fact that the saddle singular point is an intersection point of the following curves: $D(\boldsymbol{\sigma}) = 0$, $N_i(z, \boldsymbol{\sigma}) = 0$ (as shown in Fig. 1 or Fig. 2). In fact, the main determinant of the system of equations (14) D is not explicitly dependent on the spatial coordinate z. It depends on the components of the vector $\boldsymbol{\sigma}$. However, the solution of the initial-value problem determines value distributions of the components along the nozzle (Fig. 1) and thus it assigns a spatial coordinate for each value of D. Therefore, the points at which $D = 0$ can be presented (in any $\sigma_i - z$ plane) as curve $D(\boldsymbol{\sigma}(z)) = 0$ consisting of turning points that belong to different trajectories (e.g. point G and H in Fig. 2).
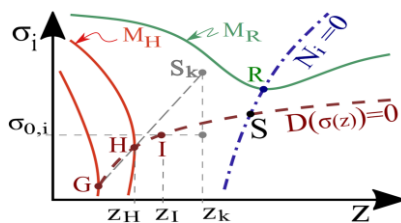
Fig. 2. Illustration of the singular saddle point S determination.

As a result of conducting the PIF algorithm, a set of trajectories is obtained. Each trajectory can be recognized as an IF or a PF trajectory (as explained earlier). However, to perform the considered procedure, only one last-found PF trajectory (green

solid line in Fig. 2) and two last-found IF trajectories (red solid lines in Fig. 2) are required. Nevertheless, the PIF algorithm must be conducted at least to the iteration in which the turning point spatial coordinate of the last-found IF trajectory is not lower than the nozzle throat coordinate ($z_H \geq z_T$). The mentioned trajectories, together with the channel geometry, determine the related mass flow rates. The necessary two of them are presented in Fig. 2, namely, M_H and M_R.

Determination of the saddle singular point approximation requires the following steps:

1. Approximate the curve $D(\boldsymbol{\sigma}) = 0$ by the straight line passing through points G and H.
2. Determine a point $S_k(z_k, \sigma_k)$ that lies on the line. At this point $z_k = z_H + \Delta z$.
3. Take $M_i = M_H + \Delta z(M_R - M_H)/(z_R - z_H)$.
4. Use the gradient descent method (take $\boldsymbol{\sigma}_k = [\sigma_{k,1}, \ldots, \sigma_{k,n}]$ as a starting point) to determine $\boldsymbol{\sigma}_0 = [\sigma_{0,1}, \ldots, \sigma_{0,n}]$ for which $D = 0$ but keep $w\rho = M_i/A(z_i)$ at each step of this method.
5. Determine z_I that satisfies the mass conservation equation: $A(z_I) = M_i/[\rho(\boldsymbol{\sigma}_0) \cdot w(\boldsymbol{\sigma}_0)]$. Point I($z_I$, $\boldsymbol{\sigma}_0$) lies on the approximation of the $D(\boldsymbol{\sigma}_0) = 0$ curve.
6. If all N_i at point I have different signs than in point H, then repeat the previous steps with smaller Δz until the required accuracy is reached (if the accuracy is reached, I is the sought approximation of the singular saddle point S). Otherwise, go to the first step but replace G with H and H with I.

The gradient descent method (also called the steepest descent method) is a first-order iterative optimisation algorithm for finding the minimum of a function [32]. However, here the algorithm was used to find $\boldsymbol{\sigma}_0$ at which $D = 0$. This is based on the fact that between the starting point where $D > 0$ and the point where D has a negative minimum value there is a point at which $D = 0$.

The proposed method is generalised in the sense that it may be applied for any model described by Eq. (14) regardless of the equations number. The singular point found by means of the above algorithm corresponds to certain inlet conditions. Those conditions may be thought as the better approximation of the original inlet conditions (Fig. 1, point B) since points G and H are located close to point S. In other words, the higher the number of PIF iterations, the better the accuracy of the solution.

4.2. Determination of a vector tangent to the transonic trajectory at the singular point

Figure 3 shows the points L, N, P that are inflection points of the subsonic trajectories. Each of the vectors: V_L, V_N, V_P is tangent to a trajectory at a corresponding inflection point. The points M, O, R represent local pressure minima. It is worth noticing that the closer to point S the subsonic trajectory lies, the closer the inflection point of this trajectory is to the pressure minimum point of this trajectory. Finally, at the transonic trajectory those points merge together into point S. Consequently, the direction of V_1 can be approximated by the direction of V_P. Thus, to perform the considered procedure, only the last-found (by the PIF algorithm) PF trajectory is required. The higher the number of

Fig. 3. Projection of the solutions to the initial-value problem on plane $p-z$ and vectors tangent to PF trajectories at inflection points.

PIF iterations, the smaller the distance between points R and S and the better accuracy of the V_1 direction approximation.

The direction of V_P can be directly used to carry out the integration "from" the found saddle singular point giving an approximation (B-P-P'-E$_1$') of the subsonic and supersonic parts of the sought transonic trajectory. Nevertheless, the higher accuracy can be reached by using V_P as a first guess for well-known iterative methods of eigenvector determination, e.g. the inverse power method [32].

The topological considerations revealed that it is impossible to start integration strictly from the singular point. Thus, it is now necessary to clarify the previously used mental shorthand: integration "from" the singular point.

Making a step (either upstream or downstream) along V_1 (or its approximation) determines a point that is eligible for starting numerical integration. The up-stream integration when it reaches z_B, determines the inlet conditions corresponding to the considered singular saddle point. Similarly, down-stream integration determines the outlet conditions. Therefore, the described procedure is a solution to an initial-value problem of the system of equations (16) with initial values: $z = z_S$ and $\sigma = \sigma_S$.

5. Proposition of after-shock trajectory determination approach

Oblique shocks, expansion waves, and complex shock interactions require at least 2D modelling to be fully represented. Mostly because they involve strong changes in both the magnitude of flow variables and the flow direction. However, since normal shock waves are perpendicular to the flow direction and cause abrupt changes in flow properties (such as pressure, temperature, density and velocity) without a flow direction change, they can be captured in 1D modelling. A normal shock wave forms when the supersonic flow decelerates to subsonic speed. In a convergent-divergent nozzle, this type of shock typically appears near the throat in the divergent section.

Figure 4 depicts a transonic trajectory (S-1-E$_1$) consisting of the subsonic part (on the left side from point S) and the supersonic part (on the right side from point S). A normal shock can theoretically occur at any point along the supersonic portion of

the trajectory (for example at an arbitrary point 1) and the already mentioned jump from the supersonic to subsonic speed must satisfy the conservation of mass, momentum and energy (or in other words the Rankine-Hugoniot relations). For the initial point 1, infinitely many possible subsonic states satisfy the required conditions.

Fig. 4. Normal shock wave in 1D modelling.

However, an assumption that the jump is associated with the lowest possible entropy generation determines state 2 (that lies on the curve $D = 0$, Fig. 4) as the final (after-shock) state. Downstream integration of the system of Eqs. (16) from this state yields a subsonic after-shock trajectory depicted as the blue line in Fig. 4. However, to integrate toward the outlet section the sign of the integration step size dl must be chosen such that $Ddl > 0$. It is worth emphasizing that the brown line segment on the left side of S is distinct from the segment on the right side, even though the condition $D = 0$ is satisfied on both sides. Each point on the left part corresponds to a different mass flow rate, while the points on the right side are associated with a constant mass flow rate, specifically that of the transonic trajectory (S-1-E$_1$).

Figure 5 presents the flowchart for the point 2 determination algorithm. The blocks in the orange frame are the implementa-

Fig. 5. Flow chart of after-shock fluid state determination approach.

tion of the Rankine-Hugoniot relations. The values of ε_ρ and ε_D determine the accuracy of the solution.

The blocks describing how to calculate y_2 and ρ_2' are correct only for the DEM but with appropriate modifications, the algorithm can be used with other models.

Figure 4 illustrates that, for a constant mass flow rate (represented by the specific brown curve), changes in the flow variables due to the jump depend on the spatial coordinate as well as the shape and orientation of the curve.

6. Implementation of the solution procedures

The methods proposed in this article, along with the author's improvements to the PIF algorithm, the model of metastable liquid properties and the Lockhart-Martinelli model were integrated into the described procedure for solving the initial-value problem and implemented in C++. The water properties were determined using library functions from the CoolProp program [33].

7. Results and discussion

The primary objective of this section is to verify the correctness of the proposed fast TTD method. Therefore, differences between the solutions determined using the proposed method and those obtained with the WAHA code are presented. Experimental data on the simulated flows are provided mostly as evidence that the simulated flows are indeed transonic. Consequently, the degree of convergence between the simulation results (obtained with the fast TTD method) and the experimental

data is insignificant (experimental validation of the DEM is not the purpose of this article). The comparison between experimental data depicting shock waves and the results obtained from the proposed shock wave modelling approach serves solely as a proof of concept, employed here due to the lack of other verification methods.

7.1. Verification of the fast transonic trajectory determination approach

Simulation result quality depends on the model chosen and the methods applied to obtain these results, and it should always be assessed through experimental validation. However, to verify the solution method (or its part), it is essential to compare its results with those obtained from another, ideally unquestionable, solution method using the same model, submodels and flow cases. Therefore, to verify the correctness of the proposed fast TTD method, simulation results of the WAHA code using the DEM model were chosen. Those results refer to selected flow cases of the Moby Dick experiment. Only cases exhibiting unquestionable shock waves have been considered, as these undeniably represent instances of transonic flow. From these cases, only those with a high probability of being normal shock waves were selected. As previously explained, the closer a shock wave forms to the nozzle throat, the more it resembles a 1D capturable shock wave (a normal shock wave). However, if the shock occurs too close to the throat, the supersonic trajectory segment is too short for adequate method verification. The cases that best meet the described requirements were used to verify the method and are presented in Figs. 6−8.
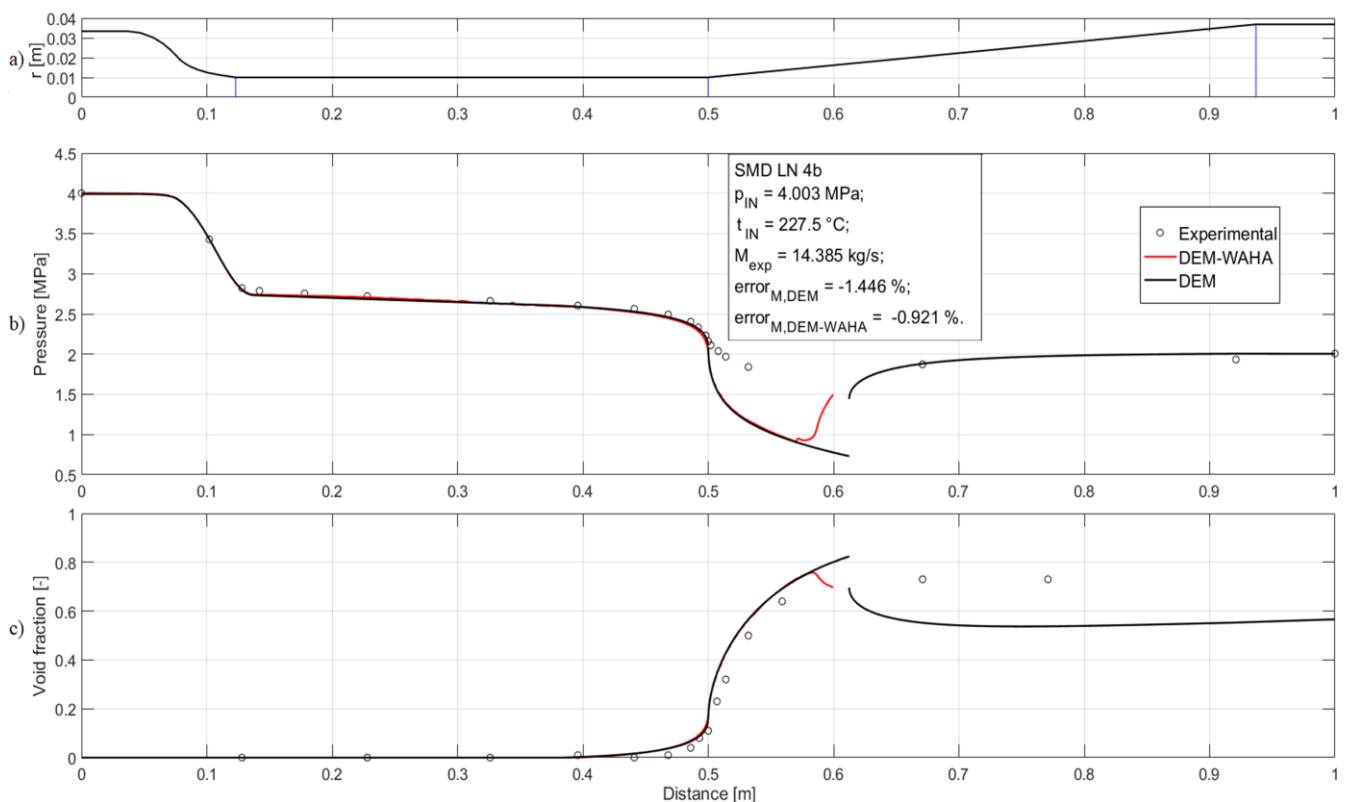
Fig. 6. Verification of the proposed TTD method by comparison with simulation results obtained from the WAHA code. Moby Dick experiment, flow case 4b: a) the experimental nozzle geometry (r – channel radius); b) the absolute static pressure distribution; c) the void fraction distribution.
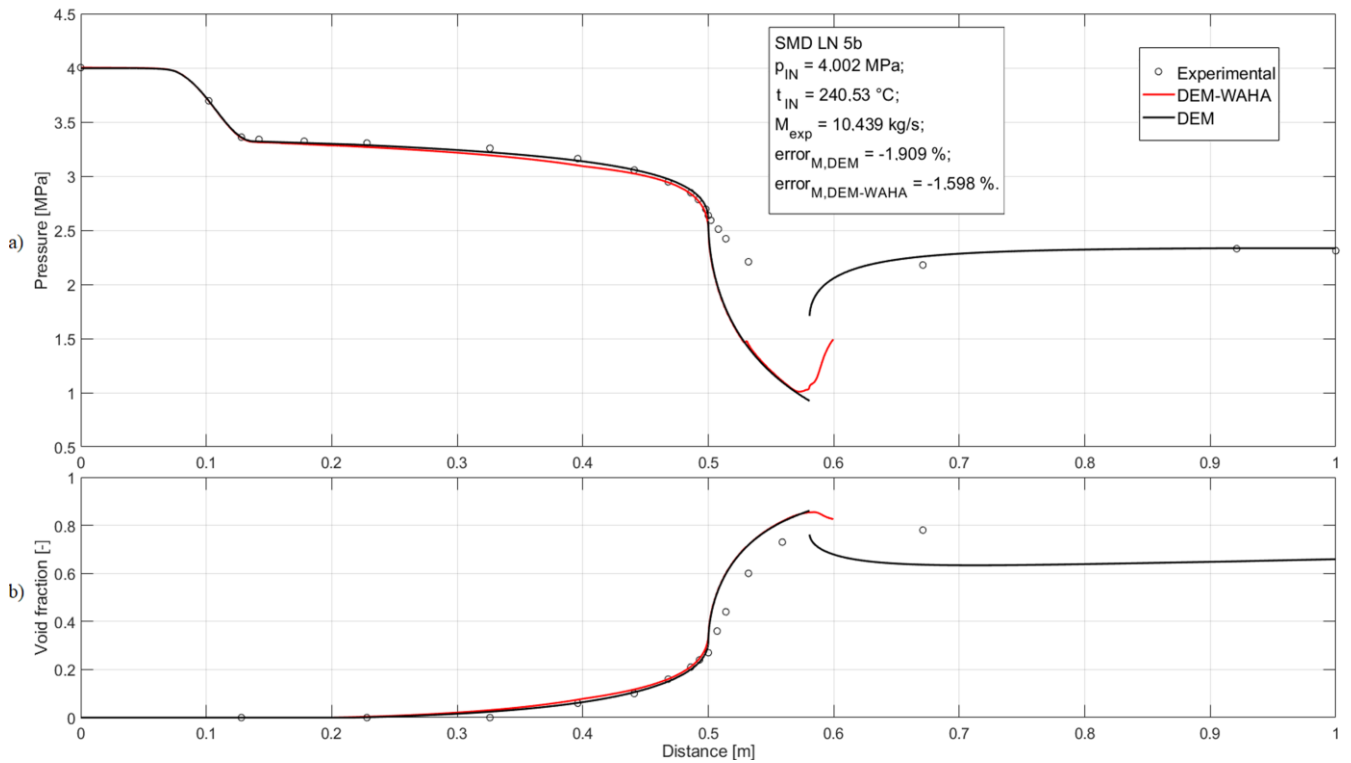
Fig. 7. Verification of the proposed TTD method by comparison with simulation results obtained from the WAHA code. Moby Dick experiment, flow case 5b: a) the absolute static pressure distribution; b) the void fraction distribution.
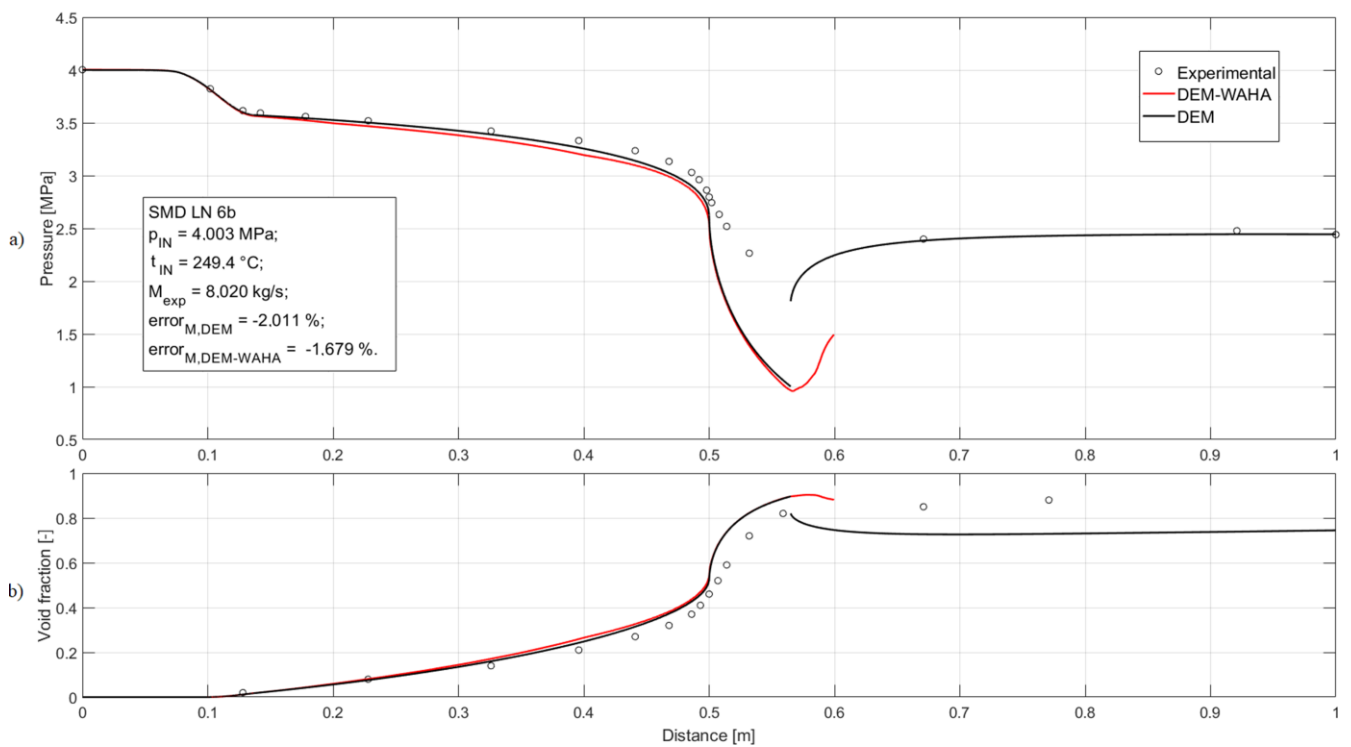
Fig. 8. Verification of the proposed TTD method by comparison with simulation results obtained from the WAHA code. Moby Dick experiment, flow case 6b: a) the absolute static pressure distribution; b) the void fraction distribution.

The WAHA code is designed to model the behaviour of shock waves and other complex flow phenomena in high-speed flows. It uses a time-dependent 1D six equation two-fluid model. The authors of the article [8] implemented the DEM using the functionality of the WAHA code and subsequently simulated the flow cases of the Moby Dick experiment. They ob-

tained results through the asymptotic convergence of the unsteady solutions to the steady-state solution. Due to the high time consumption of this method, they restricted their calculations to the nozzle cut at a distance $z = 0.6$ m from the inlet cross-section (the experimental nozzle geometry is illustrated in Fig. 6a) assuming that the absolute static pressure at this new outlet cross-section is a fraction of the pressure at the nozzle inlet:

$$p(z = 0.6 \text{ m}) = 0.37\, p_{IN}. \tag{18}$$

Those calculations resulted in data describing water transonic flows with a shock wave (Figs. 6−8, the red lines).

For each of the three selected flow cases, the absolute static pressure distribution (shown in Figs. 6b, 7a and 8a) and the void fraction distribution (shown in Figs. 6c, 7b and 8b) along the nozzle are presented.

In all cases, the inlet pressure is nearly identical ($p_{IN} \approx$ 4 MPa), while the inlet temperatures differ. In case 4b, the liquid entering the nozzle is the most subcooled, whereas in case 6b, it is the least subcooled. This is reflected in the void fraction distributions (for both simulations and experimental data): in case 6b, the void fraction rises above zero at the smallest distance from the throat ($z_{exp} \approx 0.12$ m), while in case 4b this occurs at the largest distance ($z_{exp} \approx 0.45$ m). The initial perfect convergence of the calculated void fraction distributions (the black and red lines) confirms that the same condition for the onset of nucleation was applied in both simulations, Eq. (13).

In all cases, the differences between the two simulations are meaningful for the verification only up to $z \approx 0.52$ m. From this cross-section onward, the shock waves predicted by DEM-WAHA have a rapidly increasing impact on the preceding parts of the red trajectories. In the proposed steady flow approach marked with DEM (the black line), the shock wave does not influence the trajectory in front of it (this is a direct consequence of the features of the proposed method and can be seen in all figures as a discontinuity of the black line). In the case of the unsteady asymptotic approach (DEM-WAHA), this influence is present due to the nature of the applied solution method: the asymptotic convergence never fully captures the discontinuity (in other words, accurately reflecting this discontinuity would require an infinitely long computation time). Therefore, the discrepancy between the solutions being compared, introduced by the DEM-WAHA shock waves, should not be included in the verification process. This can be easily accomplished by analysing only the differences between DEM and DEM-WAHA distributions before $z = 0.52$ m. Such comparison is shown in Fig. 9. The relative discrepancy between pressure predictions for a cross-section located at a distance z from the nozzle inlet was calculated as follows:

$$\Delta_p(z) = \frac{p_{DEM-WAHA} - p_{DEM}}{p_{DEM-WAHA}}\, 100. \tag{19}$$

Figure 9 indicates that the maximal absolute discrepancy for all flow cases appears near the nozzle throat ($z_T = 0.5$ m). However, the absolute relative discrepancy in the worst-case scenario (flow case 4b) is slightly less than 9%. The analogue verification was conducted based on the comparison of void fraction distributions. However, for the article conciseness, it is not presented.
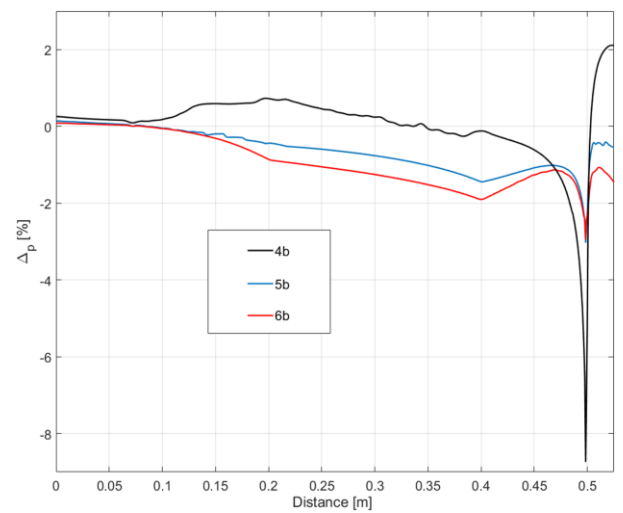
Fig. 9. Distribution of the relative discrepancy between pressure predictions, see Eq. (19).

The author decided it is sufficient to mention that the relative discrepancy in void fraction distributions is calculated in the following way:

$$\Delta_\alpha(z) = \frac{\alpha_{DEM-WAHA} - \alpha_{DEM}}{\alpha_{DEM-WAHA}}\, 100, \tag{20}$$

and achieves the maximal absolute value of approximately 6% also in case 4b.

The nature of the flows considered is such that pressure decreases monotonically until a shock wave occurs. Consequently, the denominator in Eq. (19) also decreases. This means that even if the pressure difference in the numerator (and thus the error) remained constant, the relative error would still increase. Therefore, it should be acknowledged that the relative error calculated using Eq. (19) is unfavourable for the positive verification of the proposed method, although it remains below 10%. The more favourable relative error can be obtained by putting in the denominator of Eq. (19) a mean pressure of the process ($p_{mean} \approx$ 2.37 MPa), then the absolute maximal relative discrepancy is around 7%. Even more favourable is putting in the denominator the inlet pressure, then the absolute maximal relative discrepancy is around 4.2%.

In the author's opinion, these facts lead to the conclusion that the correctness of the fast TTD method is positively verified.

It is worth noting that Fig. 9, before $z = 0.45$ m, shows oscillations − or rather noise, particularly in cases 4b and 5b − and refractions, which are most noticeable in cases 6b and 5b. The noise on the right side of Fig. 9 may stem from the shock wave predicted by the DEM-WAHA model. However, the mentioned noise observed on the left side appears exclusively in the sections associated with single-phase flows (before the nucleation onset). The author suspects that to accelerate the DEM-WAHA calculations, a single precision was used in those sections, which likely contributed to the observed noise. The mentioned refractions are due to differences in the spatial discretization of the nozzle geometry. For all presented flow cases, DEM-WAHA uses the same spatial discretization (in the range shown in Fig. 9, this consists of 693 intervals, each 0.75 mm long). In contrast, DEM, using the proposed methods, operates with an adaptive

integration step, resulting in a different spatial discretization for each flow case (that is not uniform also along the nozzle). Within the mentioned range, case 4b required the fewest intervals (3 028), while case 6b required the most intervals (5 659). The author believes that if DEM-WAHA calculations were performed with identical discretization, for each case, as that applied in DEM, the discrepancy between the simulations would be even smaller than those presented above.

7.2. Verification of after-shock trajectory determination approach

In Figs. (6)−(8), experimental data (represented by circles) show absolute static pressure distributions. In all flow cases, a monotonic pressure drop is observed up to $z = 0.532$ m. However, for all cases considered, the next data point at $z = 0.671$ m shows a pressure higher than that at $z = 0.532$ m. The substantial distance between these points, along with the convex shape formed by the four points, preceding the point at $z = 0.532$ m, indicates the presence of a shock wave between $z = 0.532$ m and $z = 0.671$ m. The flows are therefore transonic: the fluid velocity increases monotonically from the inlet to the cross-section slightly downstream of the throat, where it passes through the value of the local speed of sound and then in the divergent nozzle part (somewhere between $z = 0.532$ m and $z = 0.671$ m) the velocity decreases to a value lower than the local speed of sound.

The above-mentioned figures also present the distributions of void fraction, experimental critical mass fluxes and the error associated with each simulation in predicting these fluxes. This error was calculated as follows:

$$\text{error} = \frac{Mexp - Mcalc}{Mexp}\, 100. \tag{21}$$

It is evident that each of the simulations, thus DEM itself, predicts the pressure distributions and void fractions accurately up to the nozzle throat ($z = 0.5$ m). However, the pressure drops beyond the throat are highly overestimated, leading to an overestimation of the void fractions in the associated region.

The predicted shock waves in Figs. (6)−(8) are represented by the discontinuities in the black lines. It can be seen that the subsonic trajectories behind these discontinuities align well with the last three experimental pressure points in each of the flow cases. However, this alignment does not validate the proposed method: the relatively flat trajectories predicted by DEM in this region, make it easy to adjust the jump (discontinuity) location to achieve a trajectory that matches the mentioned points but the experimental void fraction distribution is not well approximated by this trajectory. This demonstrates that the implemented DEM is not capable of accurately describing the shock wave, which is not surprising given that Eq. (7) was developed based on data that only capture the distributions up to the throat − specifically related to flashing − and therefore does not account well for condensation that is caused by the shock wave and for the influence of the diffuser geometry on the following subsonic flow.

If these trajectories accurately described both the void fraction and pressure distributions, it would imply that DEM together with the proposed method are effective for predicting normal shock waves. Unfortunately, this is not the case; thus,

the presented data can only serve as proof of concept. They demonstrate that the method has been implemented and utilized with DEM. Moreover, the results obtained do not reveal any errors or inconsistencies in the method.

8. Conclusions

The proposed fast method for determining transonic trajectories is competitive with traditional, time-consuming approaches (such as the Newton Critical Point method or the asymptotic convergence of time-dependent solutions). The novelty of the proposed method lies in leveraging the well-known fast PIF algorithm to confine the phase space region, enabling the application of the author's (new) techniques for identifying the saddle singular point and determining the trajectory passing through it. The author also enhanced the PIF algorithm to achieve greater speed and ensure compatibility with the proposed approaches. This paper not only provides a mathematical description of the method but also offers a computational verification: a confrontation of results obtained by application of the mentioned method with results obtained from the well-known WAHA, utilizing DEM. The maximum absolute pressure discrepancy between the compared simulations (calculated conservatively) was less than 9%, which the author considers sufficient to prove the correctness of the method. This method can be applied to models as complex as DEM (such as HRM) as well as to simpler models (such as HEM and Isentropic Homogeneous Equilibrium model).

The presented analysis regarding the proposed normal shock wave modelling serves as proof of concept: the proposed method has been successfully implemented and it operates with DEM (however it can be used also with HRM, HEM and Isentropic Homogeneous Equilibrium model). Furthermore, the results obtained do not indicate any inconsistencies in the method. In the case of this method, the novelty is its implementation-oriented description that allows for easy implementation for all the above-mentioned models. Moreover, for DEM, such a method was never applied before this work. Thus, the presented results are unique.

For transonic flow with a constant mass flow rate, variations in flow variables across the shock depend on both the spatial location of the shock and the shape and orientation of $D = 0$ curve. The latter is influenced by the type of two-phase flow model applied.

After comparing the simulation results with experimental data, it has become clear that together with the implemented DEM, the proposed method is unable to accurately describe the shock waves: it can provide a precise representation of the pressure distribution behind the shock wave, but the corresponding void fraction distribution is significantly underestimated compared to the experimental data. The author thinks that this discrepancy partially arises from the application of Eq. (7), which was developed based on data that only consider distributions of flow variables up to the throat and does not adequately account for the condensation induced by the shock wave. However, also the proposed algorithm of the after-shock trajectory determination can be responsible as it assumes that the jump (shock) is associated with the lowest possible entropy generation. Thus,

the resulting following shock void fraction is lower than this caused by higher entropy generation. In the future, the contributions of each of these mechanisms should be thoroughly investigated and modelled accordingly. Finally, as the least probable reason, it should be pointed out that, contrary to the assumption adopted, the analysed waves may not be normal shock waves but oblique shock waves. In such a case, neither the presented modelling nor the measurement techniques used in the experiment are sufficient to describe and capture this phenomenon.

Finally, it is important to summarize the key advantages and limitations of the proposed methods. The disadvantages are relatively few, with the most significant being the need to develop a custom implementation of the calculation procedures described. While existing numerical libraries (available for many programming languages) can assist in this process, it remains a labour-intensive task that requires both programming expertise and the ability to apply numerical methods to simulate flow phenomena effectively. Integrating the proposed methods into commercial solvers such as Fluent of the ANSYS environment seems to be possible by using the User-Defined Function functionality. Probably the biggest advantage of such an implementation would be the possibility of using a user-friendly (graphical) interface when defining the boundary conditions of the simulation and performing calculations. However, the author anticipates that the biggest advantage of the presented procedures, namely the short computation time, may be compromised in such an implementation. The second major limitation is that the proposed procedures cannot be extended to determine time-dependent solutions. Consequently, these methods are not suitable for modelling unsteady flow. However, it is important to note that any unsteady flow model must first be validated against its steady-state version, for which the presented methods are indispensable.

The primary advantage of the described methods lies in their exceptional speed, making them suitable for incorporation into more complex, multi-stage, and multi-iterative analyses. Another significant benefit is that the solutions produced are considerably smoother than those obtained using the WAHA code. This smoothness simplifies interpretation of the results, as potential irregularities or non-monotonic behaviour in the trajectory are more likely to reflect actual phenomena rather than artefacts of the solution method. Furthermore, if doubts about the results arise, the high computational efficiency of these methods allows for easy repetition with a substantially increased number of steps, which would be far more challenging with conventional approaches.

Another major advantage is that, outside the vicinity of the singular saddle point, the methods enable dynamic adjustment of the integration step size. This feature enables acceleration of the calculations for specific flow channel geometries (pipes, slowly changing cross-section area channels) while making it possible to enhance the accuracy in areas where geometry remains unchanged, but the onset of nucleation requires a reduction in the integration step.

References

[1] Bilicki, Z., & Kestin, J. (1990). Physical aspects of the relaxation model in two-phase flow. *Proceedings of the Royal Society of London A: Mathematical, Physical and Engineering Sciences*, 428(1875), 379–397. doi: 10.1098/rspa.1990.0040

[2] Bilicki, Z., Dafermos, C., Kestin, J., Majda, G., & Zeng, D.L. (1987). Trajectories and singular points in steady-state models of two-phase flows. *International Journal of Multiphase Flow*, 13(4), 511–533. doi: 10.1016/0301-9322(87)90019-X

[3] De Sterck, H. (2007). Critical Point Analysis of Transonic Flow Profiles with Heat Conduction. *SIAM Journal on Applied Dynamical Systems*, 6(3), 645–662. doi: 10.1137/060677458

[4] Yee, H.C. (1994). Basins of attraction and the time-dependent approach to obtaining steady-state numerical solutions. In *Numerical Methods for Fluid Dynamics* (pp. 135−162). Oxford Academic. doi: 10.1093/oso/9780198536963.003.0009

[5] Angielczyk, W., Śmierciew, K., & Butrymowicz, D. (2019). Application of a fast transonic trajectory determination approach in 1-D modelling of steady-state two-phase carbon dioxide flow. *E3S Web of Conferences*, 128, 06005. doi: 10.1051/e3sconf/201912806005

[6] Seynhaeve, J.M., & Giot, M. (2004). The WAHA code: a numerical tool for water hammer in two-phase flow - some simulations of experiments. *117. session of the scientific and technical committee of the French hydro-technical society „Advances in the modelling methodologies of two-phase flows"*, 24-26 November, Lyon, France.

[7] Banaszkiewicz, M., & Kardaś, D. (1997). Numerical Calculations of the Moby Dick Experiment by Means of Unsteady Relaxation Models. *Journal of Theoretical and Applied Mechanics*, 35(2), 211−232.

[8] Bartosiewicz, Y., & Seynhaeve, J.M. (2013). Delayed Equilibrium Model (DEM) of Flashing Choked Flows Relevant to LOCA. *Multiphase Science and Technology*, 25(2–4), 117–131. doi: 10.1615/MultScienTechn.v25.i2-4.50

[9] Bartosiewicz, Y., Giot, M., & Seynhaeve, J.M. (2010). Revisiting Modeling Techniques and Validation Experiments for Two-Phase Choked Flows Relevant to LOCA. (2010). *The 8th International Topical Meeting on Nuclear Thermal-Hydraulics, Operation and Safety (NUTHOS-8) N8P0317*, 10–14 October, Shanghai, China.

[10] Emanuel, G. (1964). A general method for numerical integration through a saddle-point singularity with application to one-dimensional nonequilibrium nozzle flow. *Technical documentary report no. AEDC-TDR-64-29*. Stanford University, California, USA.

[11] De Sterck, H., Rostrup, S., & Tian, F. (2009). A fast and accurate algorithm for computing radial transonic flows. *Journal of Computational and Applied Mathematics*, 223(2), 916–928. doi: 10.1016/j.cam.2008.03.019

[12] Cheng, K., Meng, T., Zhao, F., & Tan, S. (2019). Development and validation of a thermal hydraulic transient analysis code for offshore floating nuclear reactor based on RELAP5/SCDAPSIM/MOD3.4. *Annals of Nuclear Energy*, 127, 215–226. doi: 10.1016/j.anucene.2018.12.004

[13] Ohnuki, A., Akimoto, H., & Murao, Y. (1993). Assessment of TRAC-PF1/MOD1 code for thermal-hydraulic behavior in pressure vessel during reflood in SCTF test with a radial power distribution. *Technical documentary report no JAERI-M--93-139*, Japan Atomic Energy Research Institute, Tokyo, Japan.

[14] Dor, I., Geffraye, G., Lavialle, G., & Mieusset, T. (2004). Recent Improvements of Physical Models in the CATHARE Code and Their Validation. 12th International Conference on Nuclear Engineering, Proceeding Paper (pp. 681–691), 25−29 April, Arlington, Virginia, USA. doi: 10.1115/ICONE12-49408

[15] Sánchez, V.H., Thieme, M., & Tietsch, W. (2012). Validation and Application of the Thermal Hydraulic System Code TRACE for Analysis of BWR Transients. *Science and Technology of Nuclear Installations*, 2012(1), 247482. doi: 10.1155/2012/247482

[16] Gale, J., Tiselj, I., & Horvat, A. (2008). Two-fluid model of the Waha code for simulations of water hammer transients. *Multiphase Science and Technology*, 20(3–4), 291–322. doi: 10.1615/MultScienTechn.v20.i3-4.40

[17] Va, B., Lee, W.-T., & Roe, P. (1991). Characteristic time-stepping or local preconditioning of the Euler equations. *10th Computational Fluid Dynamics Conference*. 24−26 June, Honolulu, USA. doi: 10.2514/6.1991-1552

[18] Angielczyk, W., Seynhaeve, J.M., Gagan, J., Bartosiewicz, Y., & Butrymowicz, D. (2019). Prediction of critical mass rate of flashing carbon dioxide flow in convergent-divergent nozzle. *Chemical Engineering and Processing - Process Intensification*, 143, 107599. doi: 10.1016/j.cep.2019.107599

[19] Angielczyk, W., Bartosiewicz, Y., & Butrymowicz, D. (2020). Development of Delayed Equilibrium Model for CO2 convergent-divergent nozzle transonic flashing flow. *International Journal of Multiphase Flow*, 131, 103351. doi: 10.1016/j.ijmultiphaseflow.2020.103351

[20] Angielczyk, W. (2024). A Review of the Relaxation Models for Phase Transition Flows Centered on the Topological Aspects of the Nonequilibrium Mass Transfer Modelling. *Acta Mechanica et Automatica*, 18(3), 526–535. doi: 10.2478/ama-2024-0056

[21] Nakagawa, M., Berana, M.S., & Kishine, A. (2009). Supersonic two-phase flow of CO2 through converging–diverging nozzles for the ejector refrigeration cycle. *International Journal of Refrigeration*, 32(6), 1195–1202. doi: 10.1016/j.ijrefrig.2009.01.015

[22] Gale, J., & Tiselj, I. (2004). Simulation of the Critical Flashing Flow with the Transient 1D Two-Fluid Model. *ASME 2004 Heat Transfer/Fluids Engineering Summer Conference*. 11−15 July, Charlotte, North Carolina, USA. doi: 10.1115/ht-fed2004-56315

[23] Ebrahimzadeh Azghadi, F. E., Mahpeykar, M.R., Pasandideh Fard, M., & Lakzian, E. (2022). Numerical simulation of nucleating flow and shock capturing in steam turbines by a simple low-dissipation upwind scheme using an Eulerian-Lagrangian model. *Computers & Fluids*, 249, 105699. doi: 10.1016/j.compfluid.2022.105699

[24] Gaballa, H., Jafari, S., Di-Lella, A., Habchi, C., & de Hemptinne, J.C. (2022). Thermodynamics analysis of CO_2 condensation in supersonic flows for the potential of clean offshore natural gas processing. *Applied Energy*, 320, 118523. doi: 10.1016/j.apenergy.2022.118523

[25] Chen, Z., & Liu, G. (2024). Analysis of the Internal Flow Features of a CO_2 Transonic Nozzle and Optimization of the Nozzle Shape Profile. *Applied Thermal Engineering*, 243, 121945. doi:10.1016/j.applthermaleng.2023.121945

[26] Seynhaeve, J.-M., De Crécy, A., & Bartosiewicz, Y. (2015). Uncertainty analysis of delayed equilibrium model (DEM) using the CIRCE methodology. *NURETH-16, Chicago, IL, August 30-September 4* (pp. 1143−1156).

[27] Attou, A., Bolle, L., & Seynhaeve, J.M. (2000). Experimental study of the critical flashing flow through a relief line: evidence of the double-choked flow phenomenon. *International Journal of Multiphase Flow*, 26(6), 921–947. doi: 10.1016/S0301-9322(99)00077-4

[28] Lorenzo, M.D., Lafon, P., Seynhaeve, J.-M., & Bartosiewicz, Y. (2017). Benchmark of Delayed Equilibrium Model (DEM) and classic two-phase critical flow models against experimental data. *International Journal of Multiphase Flow*, 92, 112–130. doi: 10.1016/j.ijmultiphaseflow.2017.03.004

[29] Skripov, V. P. (1992). Metastable states. *Journal of Non-Equilibrium Thermodynamics*, 17(3), 193–236. doi: 10.1515/jnet.1992.17.3.193

[30] Angielczyk, W. (2021). *Modelling of CO2 transonic flashing flow through a convergent-divergent nozzle using the Delayed Equilibrium Model*. PhD Thesis. Bialystok University of Technology, Faculty of Mechanical Engineering, Białystok, Poland.

[31] Bouré, J.A., Fritte, A.A., Giot, M.M., & Réocreux, M.L. (1976). Highlights of two-phase critical flow: On the links between maximum flow rates, sonic velocities, propagation and transfer phenomena in single and two-phase flows. *International Journal of Multiphase Flow*, 3(1), 1–22. doi: 10.1016/0301-9322(76)90030-6

[32] Press, W.H., Teukolsky, S.A., Vetterling, W.T., & Flannery, B.P. (2002). *Numerical Recipes in C++: The Art of Scientific Computing* (Third Edition, Vol. 1002). Cambridge University Press.

[33] Bell, I.H., Wronski, J., Quoilin, S., & Lemort, V. (2014). Pure and Pseudo-pure Fluid Thermophysical Property Evaluation and the Open-Source Thermophysical Property Library CoolProp. *Industrial and Engineering Chemistry Research*, 53(6), 2498–2508. doi: 10.1021/ie4033999